3

Theoretical Foundation and Experimentation

3.1 Introduction

Theory of Weibull model and experimentation procedures has been explained in brief in subsequent sections of this chapter. Procedure for estimation of Weibull characteristic strength, effective volume and area has been explained with unimodular and bimodular assumptions. These parameters characterize the reliability of graphite components or structures, where even two identical specimens exhibit large variability in strength. The theory related to the effect of size on the strength of graphite specimen using weakest link theory has been explained. The implementation of bimodular finite element model has been discussed in this chapter. The influence of bimodularity on failure and fracture characterizing parameters has been illustrated.

3.2 Weakest Link Theory

The use of advanced high purity graphite materials and similar ceramic materials in structural applications requiring high component integrity has led to the development of a probabilistic design methodology due to the large scatter in strength and randomness of failure behaviour. Reliability of high risk components

involving nuclear grade graphite should not be compromised and endeavors are being made to propose a sound design philosophy. Though their true nature deviates from a classical elasticity problem posing a challenge to research community, the advent of efficient computational and experimental methodology has also been progressed to tackle such complexity. Therefore, a new spectrum of bimodular probabilistic design methodology has been developed for modeling the failure and fracture behavior of such components.

The methodology combines:

(1) Fracture mechanics theory for brittle failure of bimodular materials and

(2) Weibull analysis of random failure strength data

Inherent to this design procedure is that the requirement of reliability and safety of the component be relaxed at an acceptable limit. The statistical nature of fracture in engineering materials can be conceptualized by Weibull model(Weibull 1939b) based on the weakest-link theory as originally proposed by Pierce (Peirce 1926). The weakest-link model assumes that the structure is analogous to a chain with n links. Each link may have a different limiting strength. When a load is applied to the structure such that the weakest link fails, then the structure fails. Observations show that advanced monolithic ceramics closely follow the weakest-link theory. Weibull WLT model does not consider failure caused by purely compressive stress states, because the compressive strength is much larger than the tensile strength for ceramics. Consequently, failure is predominant by tensile strength, so the compressive stresses are neglected. In other words, the compressive and tensile principal stresses in each element are compared. When principal compressive stress exceed three times the maximum principal tensile stress in a given element, compressive stress state is assume to be predominated, and the

corresponding reliability of the element is set to be one. The weakest link theory predicts size effect on the strength of structural components. The flaws or defects present in structural components depend upon the material volume or surface area. Moreover, the strength of the structural component is directly related to effective volume and effective surface area. The number of flaws in smaller component is lesser than larger components, which lead to lesser chance to fail at similar strength. That means the characteristic failure strength is lesser for larger components than smaller components. On the other hand the largest flaw present in the larger component is more critical than the smaller component. The component failure may not be initiated at maximum nominal stress zone. A large flaw may exist in a region, which is other than the nominal maximum stress region. Therefore, for accurate analysis the complete stress solution of a component is required. Multiaxial stress state behavior is not predicted by classical weakest link theory. Various concepts like Principle of Independent Action (PIA), Weibull's stress averaging, Batdorf's theory have been used to account for multiaxial stress state. In this work PIA criterion has been taken for the analysis of multiaxial stress state behavior. For understanding the basic mathematics, let us assume a stressed component containing many flaws, and assume that failure is due to any number of independent and mutually exclusive links (elements). Suppose, the infinitesimal probability of failure of each element is ΔP_f. The whole component is discretized into *n* incremental elements. Then the probability of survival of i^{th} element is

$$\left(\Delta P_s\right)_i = 1 - \left(\Delta P_f\right)_i \tag{3.1}$$

where, $(\Delta P_s)_i$ is probability of survival. The overall probability of survival of the whole component is defined as the product of the probabilities of survival individual element

$$\sum_{i=1}^{n}(\Delta P_s)_i = \sum_{i=1}^{n}\left(1-(\Delta P_f)_i\right) \tag{3.2}$$

$$\sum_{i=1}^{n}(\Delta P_s)_i \cong \sum_{i=1}^{n}\left(\exp-(\Delta P_f)_i\right) \tag{3.3}$$

$$\sum_{i=1}^{n}(\Delta P_s)_i \cong \exp\left(-\sum_{i=1}^{n}\left((\Delta P_f)_i\right)\right) \tag{3.4}$$

Consider an existence of a function $N(\sigma)$, representing the crack density function, which is defined as the number of flaws per unit volume having a strength equal to or less than uniform tensile strength (σ).The probability of failure of i^{th} element is in form of crack density function is

$$(\Delta P_f)_i = (N(\sigma)\Delta V_i) \tag{3.5}$$

where, ΔV_i is elemental volume. Expression of $(\Delta P_f)_i$ is substituted in Eq. (3.4), we get:

$$\sum_{i=1}^{n}(\Delta P_s)_i = -\exp\left(\sum_{i=1}^{n}(N(\sigma)\Delta V_i)\right) \tag{3.6}$$

Resultant probability of survival is

$$P_s = \exp\left(-\sum_{i=1}^{n}(N(\sigma)\Delta V_i)\right) \tag{3.7}$$

And overall probability of failure will be

$$P_f = 1-\exp\left(-\sum_{i=1}^{n}(N(\sigma)\Delta V_i)\right) \tag{3.8}$$

The probability of failure in integral form, the above equation is changed into

$$P_f = 1 - \exp\left(-\int_V \left(N(\sigma) dV \right) \right) \tag{3.9}$$

$$P_f = 1 - \exp(-B) \tag{3.10}$$

Where B is risk of rupture as said by Weibull(Weibull 1939b). Risk of rupture is commonly used in reliability analysis. Eq.(3.9) and (3.10) are also be applicable to characterize flaws distributed over surface, if the elemental volume and volume dependent crack density function are replaced by elemental surface area and surface area dependent crack density function.

According to Weibull distribution, crack density function is replace by three parameter power function and

$$P_f = 1 - \exp\left(-\int_V \left(\left(\frac{\sigma - \sigma_{uV}}{\sigma_{0V}} \right)^{m_V} dV \right) \right) \tag{3.11}$$

where, σ_u is threshold stress, σ_{0V} is scale parameter corresponds to the stress level where 63.21 percent of specimens with unit volumes would fracture and m_V is shape parameter or Weibull Modulus. The shape parameter is very important to characterize size effect. These Weibull parameters are material properties and it depends on environmental test conditions and processing. Threshold parameter is usually taken zero for ceramic or graphite and by eliminating the threshold stress Eq. (3.11) will be

$$P_f = 1 - \exp\left(-\int_V \left(\left(\frac{\sigma}{\sigma_{0V}} \right)^{m_V} dV \right) \right) \tag{3.12}$$

The above equation used to analyze fracture strength data from simple uniaxial specimen tests. For the analysis of the multiaxial stress state, PIA model has been based on principal stresses ($\sigma_1 \geq \sigma_2 \geq \sigma_3$), which are assumed to act independently:

$$P_f = 1 - \exp\left(-\left(\frac{1}{\sigma_{0V}} \right)^{m_V} \int_V \left(\left(\sigma_1^{m_V} + \sigma_2^{m_V} + \sigma_3^{m_V} \right) dV \right) \right) \tag{3.13}$$

In the present work, PIA model is used to estimate the size effect and the numerical approach for evaluation of effective volume and effective surface area.

3.3 Size Effect on Strength

Though size effect on strength has long been recognized with the era of Leonardo da Vinci (1452 – 1519), where he has conducted tests to determine the strength of iron wires, the scaling of design parameter, geometry and strength from one size (let us say laboratory specimen) to the prototype has been challenging enough to boost any confidence on prevailing laid down design principles. He postulated an inverse relationship between the strength and the length keeping the wire diameter constant (Timoshenko 1953). Some part translation of da Vinci's sketch book can be quoted as follows (Irwin and Wells 1965).

"Observe what the weight was that broke the wire, and in what part the wire broke… Then shorten this wire, at first by half, and see how much more weight it supports; and then make it one quarter of its original length, and so on, making various lengths, and nothing the weight that breaks each one and the place in which it breaks."

When, the results of U.S. Naval research Laboratory (1958) on the strength of glass fibers as reported in literature (Irwin 1964), corroborated the early findings of Leonardo da Vinci, one can only awe inspire the findings of what a Genius he might be to motivate further work in the field. For brevity, bimodular material behavior was not recognized and presumably at a natal stage in later years to investigate its influence on size effect and strength dependency. The problem now becomes a stress dependent elasticity phenomenon, where intriguingly, state of

stress itself becomes a function of modulus of elasticity and the former happen to be an unknown as a priori.

For design engineers, the size effect is, probably the most compelling reason for using fracture mechanics and statistical approach to deal strength of a structural component. The size effect is defined through a comparison of geometrically similar structures of different sizes, and is conveniently characterized in terms of the strength, which is same for geometrically similar structures of different sizes, then it is said to be, there is no size effect. A dependence of strength on the structural component size is called the size effect. Generally the strength of larger specimens is lesser than the smaller specimen. During actual application the strength of the structural component which might be much larger than the laboratory tested specimens, which mean the strength of structural component is significantly lower than the laboratory tested specimen. So, for design of critical component inside the reactor core of nuclear reactor, the size effect analysis is mandatory. For characterization and accurate accountability of size effect comparison between two different sizes of specimens, the concept of Weibull effective volume and effective surface area has been used. The Weibull weakest-link theory leads to a strength dependency on specimen size is

When volume flaws dominated:

$$\frac{\sigma_1}{\sigma_2} = \left(\frac{V_{E2}}{V_{E1}} \right)^{1/m_v} \tag{3.14}$$

When surface flaws dominated:

$$\frac{\sigma_1}{\sigma_2} = \left(\frac{A_{E2}}{A_{E1}} \right)^{1/m_A} \tag{3.15}$$

Where, σ_1, σ_2 are the characteristic strength of the specimen type 1 and 2; V_{E1}, V_{E2} are effective volumes of the specimen type 1 and 2; A_{E1}, A_{E2} are effective surfaces of the specimen type 1 and 2; m_V and m_A is Weibull modulus for effective volume and effective surface.

3.4 Weibull effective volume and effective surface area

Effective volume is the volume of a hypothetical tensile specimen, which, when subjected to the maximum stress has the same probability of failure as the tested specimen (flexural, C-ring, O-ring) stressed at same maximum stress. The effective volume is given by

$$V_E = \int_V \left\{ \frac{\sigma}{\sigma_{\max}} \right\}^{m_V} dV \tag{3.16}$$

where, the $\sigma_{\max}$ is maximum stress. And effective surface area is given by:

$$A_E = \int_A \left\{ \frac{\sigma}{\sigma_{\max}} \right\}^{m_A} dA \tag{3.17}$$

By using above expression (3.16) and (3.17) the effective volume and effective surface have derived respectively.

3.5 Numerical Evaluation of Effective Volume and Effective Surface Area

Experimental testing of the appropriate number of specimens of similar type has been conducted. The random variable data sets of failure strength of different size

specimens have been estimated from experimental testing. The obtained random failure data has been gone through the Weibull distribution by the help of WeibPar software. And estimation of Weibull parameter is performed. After, estimation of Weibull parameter and analytical derivation of effective volume and effective surface area, numerical estimation has been performed with help of finite element software and WeibPar and CARES life estimation software and self-developed code. Now, unimodular and bimodular finite element models have been developed for the stress analysis. Then, with the help of WeibPar and CARES, effective volume has been evaluated for unimodular material model. The unimodular finite element results file for various flexural loading condition have been incorporated as input file to the CARES-life program. The CARES natural file so generated stores the data of stress, strain, displacement, coordinates of each and every node for use in reliability analysis and effective volume calculation. The flow chart in Fig. 3.1 describes the calculation procedure of effective volume both for unimodular and bimodular specimens. The experimental unimodular strength based Weibull model using various estimators is followed by Weibpar and CARES-life analysis program (WeibPar V-4.3 and CARES V-9.3) to evaluate the effective volume employing Principal of Independent Action. The evaluated experimental based effective volume for bimodular specimens have been compared with the analytical results of unimodular specimens. However, for bimodular effective volume evaluation, program subroutines have been written to calculate the effective volume from the bimodular finite element model.

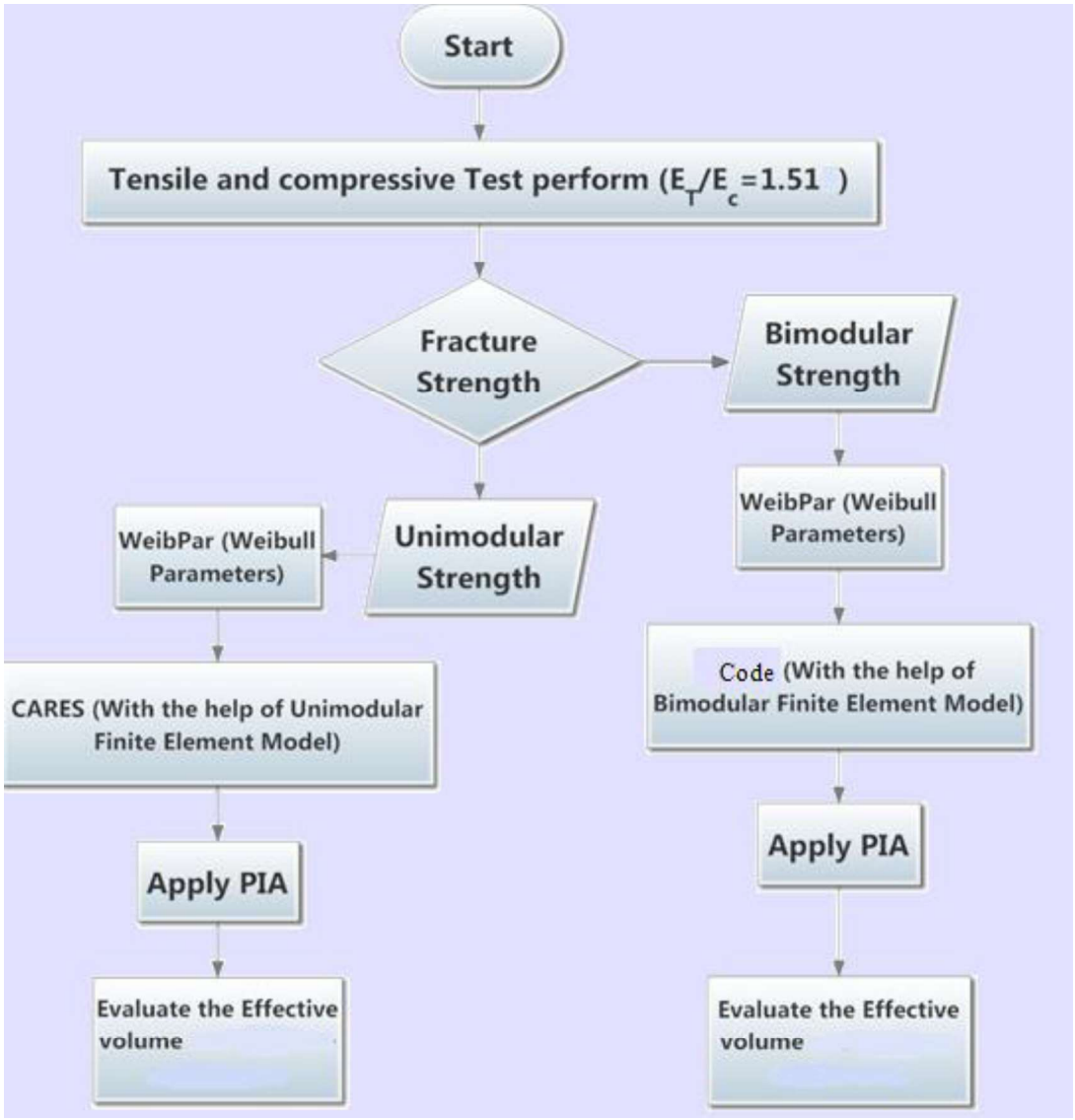

Fig. 3.1 Flow diagram to calculate the experimental based effective volume and effective surface area calculation using Weibpar and CARES in unimodular case and bimodular FE model followed by sub routine.

Bimodular strength based Weibull model has been developed using linear regression, biased maximum likelihood estimator and unbiased maximum likelihood estimator. Effective volume (bimodular) has been evaluated from the bimodular FE model using principal of independent action.

3.6 Finite Element Implementation of Bimodularity

The FE model for bimodular material is developed based on the stress-dependent elasticity concept. The linearized and non-linearized constitutive model as shown in Fig. 3.2 exhibiting different elastic moduli in tension and compression requires iterative numerical procedures for evaluating the state of stress of bimodular material specimen. The present work follows the bimodular Ambartsumyan constitutive model (Ambartsumyan 1966, 1969, Ambartsumyan and Khachatryan 1966b, a; Ambartsumyan, S.A.; Khachatryan 1966) for characterizing the bimodular strength scaling. The bimodular theory postulates the tension-compression stress-strain plots into two straight lines, whose tangents at the origin are discontinuous. This seems adequate for efficient modeling of the fracture behavior of many natural and man-made brittle materials demonstrating bimodularity.

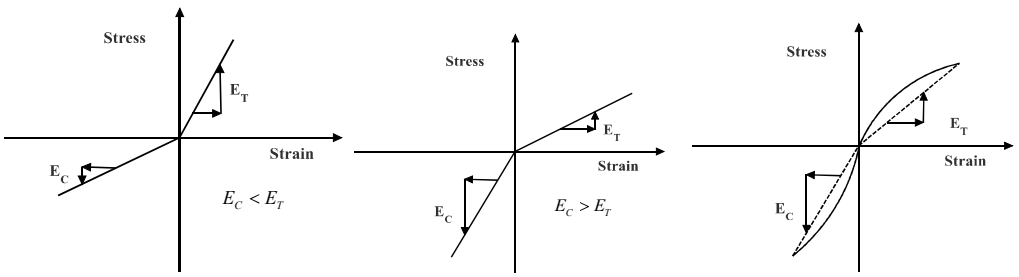

(a) (b) (c)

Fig. 3.2 Bimodular constitutive model: (a) Bilinear model when $E_T > E_C$ (b) bilinear model when $E_T < E_C$ and (c) non-linear model for actual condition

The elastic continuum mechanics approach has the assumption that the stressed body is continuous, homogeneous, and isotropic and all deformations are small enough to have theory of superposition valid for all response characteristics. The

bimodular constitutive model for tensile and compressive state of stress has been defined as

$$\varepsilon_T = \frac{\sigma_T}{E_T} \qquad \text{and } \varepsilon_C = \frac{\sigma_C}{E_C} \tag{3.18}$$

where, σ, ε, and E respectively represent the stress, strain and Young's modulus for a given material and loading configuration and subscripts 'T' and 'C' denote the constituent tensile and compressive parameters. Since the modulus of elasticity itself is a function of state of stress and the latter being an unknown as a priori; a step function approach is adopted as similar to a Dirac delta functional having a value of either one or zero depending on the state of stress. The model step function of the bilinear bimodular material for representing the stress-dependent elasticity problem can be written as

$$\varepsilon^b = \left(\left(\frac{U(\sigma^b)}{E_T} \right) + \left(\frac{U(-\sigma^b)}{E_C} \right) \right) \sigma^b \tag{3.19}$$

Where, U is a step function defined as

$$\begin{aligned} U(\xi) &= 0 \quad \text{if } \xi < 0; \\ &= 1 \quad \text{if } \xi > 0 \end{aligned} \tag{3.20}$$

The superscript b implies bimodularity; ε^b and σ^b represent the bimodular strain and stress field respectively. The constitutive model for the three-dimensional tensile state of stress is given as

$$\varepsilon_{ij}^T = a_{ijkl}^T \sigma_{kl}^T \tag{3.21}$$

and for compressive region

$$\varepsilon_{ij}^{C} = a_{ijkl}^{C} \sigma_{kl}^{C} \tag{3.22}$$

Bimodular constitutive relationship is given by

$$\varepsilon_{ij}^{b} = a_{ijkl}^{b} \sigma_{kl}^{b} \tag{3.23}$$

The flexibility coefficient tensor, a_{ijkl}^{b} for bimodular state of stress is defined as

$$a_{ijkl}^{b} = a_{ijklmn}^{T} U\left[f_{mn}(\sigma_{pq}^{b}) \right] + a_{ijklmn}^{C} U\left[-f_{mn}(\sigma_{pq}^{b}) \right] \tag{3.24}$$

ε_{ij}^{T}, ε_{ij}^{C} and σ_{kl}^{T}, σ_{kl}^{C} are strain tensor and stress tensor in tensile and compressive region respectively. a_{ijkl}^{T}, a_{ijkl}^{C} are the respective flexibility coefficient tensor in tensile and compressive state. The functions f_{mn} are the functions of state of stress. The constitutive equations so developed should satisfy the principle of coordinate invariance. Therefore, f_{mn} are independent of coordinate rotation being isotropic functions of their arguments. Hence, the function f_{mn} is expressed as an argument as follows.

$$f_{mn} = f_{mn}\left(I_1, I_2, I_3\right) \tag{3.25}$$

where, I_1, I_2 and I_3 are the well-known stress invariant of elasticity theory, which satisfy the following cubic equation.

$$\sigma^3 - I_1\sigma^2 + I_2\sigma^2 - I_3 = 0 \tag{3.26}$$

$f_{mn} = 0$ if $m \neq n$ and

$$f_{mn} = \sigma_i \text{ if } m = n \tag{3.27}$$

$f_{mn}(\sigma_{pq}) = \sigma_r$ where, r=I, II, III are the three roots of Eq. (3.26). Since the bimodular elastic constants are the functions of the sign of principal stresses, this

can be incorporated to Eq. (3.23) for defining the general form of bimodular elasticity. So we obtain

$$\varepsilon_{ij}^{b} = \left[a_{ijklr}^{T} U(\sigma_r) + a_{ijklr}^{C} U(-\sigma_r) \right] \sigma_{kl}^{b} \tag{3.28}$$

where, the ε_{ij}^{b}, σ_{kl}^{b} are the bimodular tensorial strain and stress matrix, whereas σ_r is function of principle stress. However, with reference to the principle of coordinate invariance for any arbitrary plane, the mean principal stress or octahedral normal stress σ_o is considered as a function of σ_r and the step function with reference to Eq. (3.20) is defined as follows.

$$\begin{aligned} U(\xi) \quad &= 0 \quad \text{if } \xi \left(= \frac{\sigma_1 + \sigma_2 + \sigma_3}{3} \right) < 0; \\ &= 1 \quad \text{if } \xi > 0 \end{aligned} \tag{3.29}$$

The strain tensor so developed being the function of octahedral normal stress field is expressed as

$$\varepsilon_{ij}^{b} = \left[a_{ijklo}^{T} U(\sigma_o) + a_{ijklo}^{C} U(-\sigma_o) \right] \sigma_{kl}^{b} \tag{3.30}$$

Now the above expression is incorporated in FE bimodular model. Appropriately, program subroutines have been written to incorporate the above condition in the finite element software COMSOL-multiphysics to model the stress dependent elasticity problem of crack progression behaviour iteratively. The detail of the programing flowchart has been shown in Fig. 3.3. The computational time on the server based parallel computing depends upon the tolerance accuracy of stress dependent elasticity.

The first iteration has been solved assuming the material to be isotropic and unimodular. The neutral surface and geometric symmetric mid-surface both located at the same place. Then the iteration invokes the step function to define

the bimodularity based on the sign of function 'σ_o' and then reevaluation of the state of stress is carried out. The do loop is carried forward till the convergence criteria is satisfied. The accuracy of this three-dimensional problem for determining neutral surface iteratively is very much mesh sensitive and depends on the number of sub steps for each iteration. Fig. 3.3 demonstrates this logic flow chart for the bimodular flexural problem.

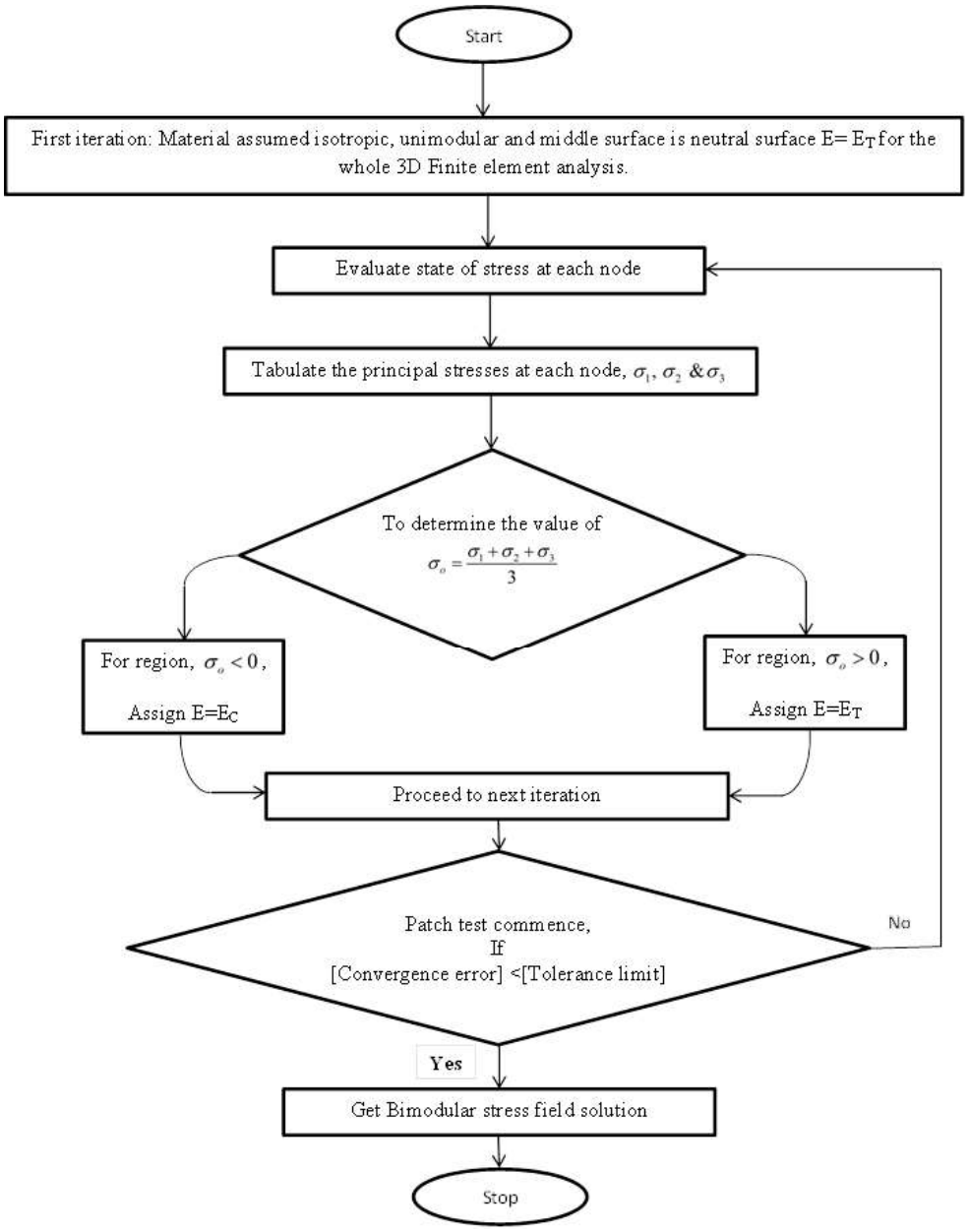

Fig. 3.3 Program flow chart for evaluation of neutral surface in a bimodular flexure specimen

The flow chart starts with location of neutral axis for taking the tensile modulus as unimodular stress field. According to the sign of the principal stress function parameter, the domain of the tensile stress filed has been identified separately from the compressive stress field for each subsequent iteration. Subsequently, the tensile and compressive modulus of elasticity is assigned to the tensile and compressive region. The bimodular effect now can be observed in the flexural simulation of the graphite specimen due to non-uniform tensile and compressive zones. In the next iteration the region of tensile and compressive zone again changes and so also the neutral axis is shifted. The procedure is repeated till a predefined tolerance limit of close to 0.001 has been achieved. The change of state of stress between two consecutive iterations if remain constant for 99.99% of the assigned nodes, then the iteration is stopped. To lessen the computational time, advantage of parallel processing has been invoked for each bimodular index. On the basis of above discussion, the bimodular finite element models for the three point and four point bend specimens have been simulated. In order to test the accuracy of finite element results, comparison needs to be made with exact analytical solutions, if available. Alternatively, as the finite element method minimizes a prescribed functional then the solution will converge to the true value with increasing mesh density and therefore, comparison of global response by mesh refinement technique is also an accepted procedure for such convergence studies.

3.7 Experimental Characterization of Bimodularity

Experimentation for tensile, compressive and fracture test data have been conducted as per relevant ASTM standards. The fracture data has been obtained by using digitalized image correlation software with continuous image capturing through high speed camera attachment to the INSTRON machine set up. The tensile and compressive specimens are prepared from the cuboidal shape graphite log of size as 1040x650x350mm^3 and cut down in the way that it occupies horizontal orientation or against the gravity as shown in Fig. 3.4. The modulus of elasticity in tension and compression has been evaluated for this sample of horizontal oriented specimens.

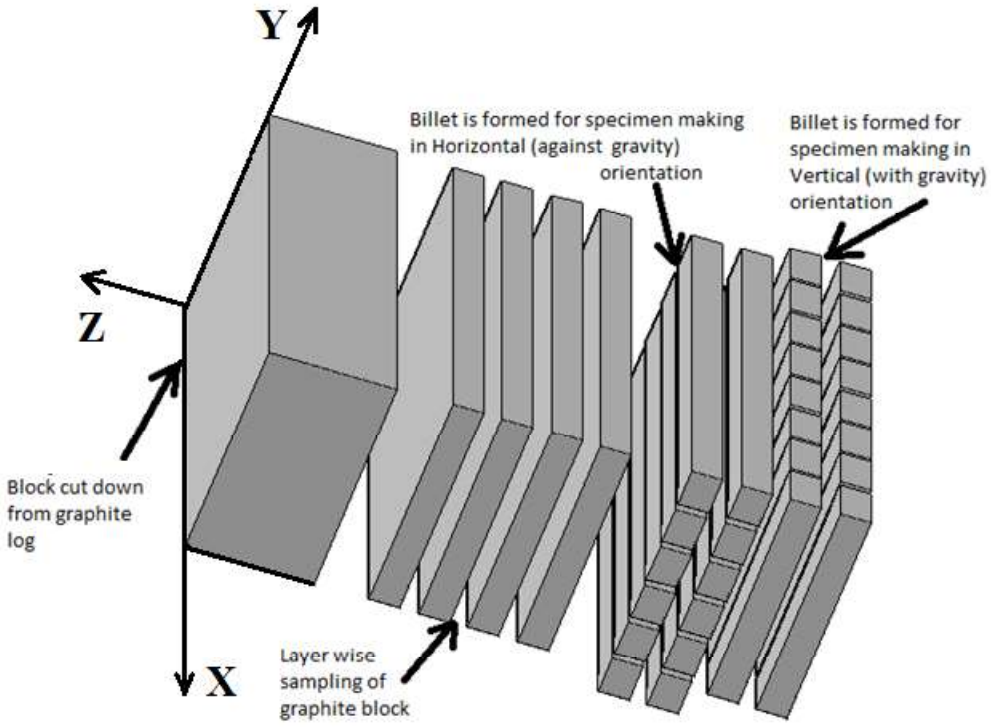

Fig. 3.4 The specimens making in the two orientations vertical (with gravity:Y-axis) and horizontal (against gravity: X-axis) within specific graphite block size 1040x650x350mm^3.

The fracture specimens are also prepared in the similar orientation according to ASTM D7779 standard (ASTM D7779-11 2011). Fracture experimentation have been conducted to determine the critical stress intensity factor and strain energy release rate for the three point single edged notched bend (SENB) specimens prepared from the same log and subjected to displacement controlled point load.

Fig. 3.5 Tensile specimen with fixture train

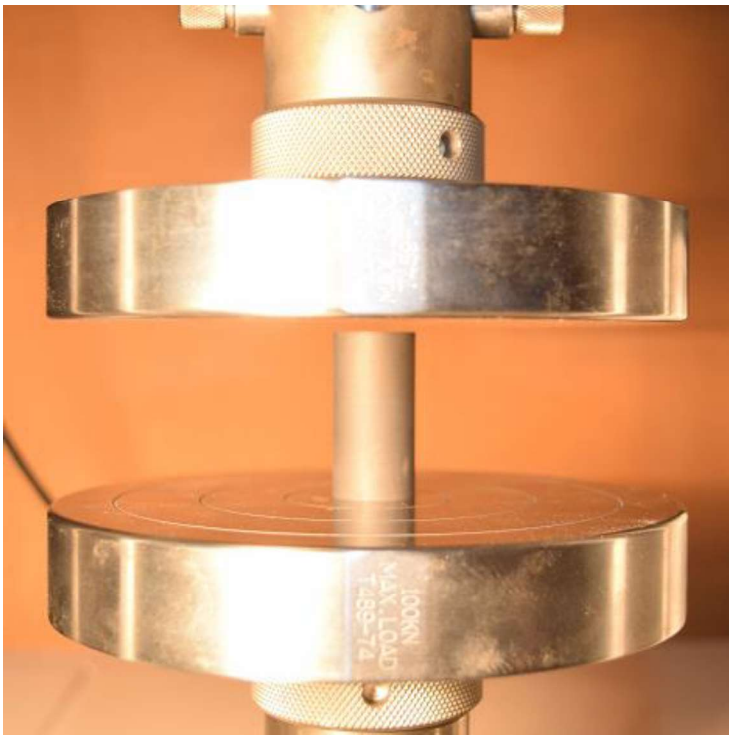

Fig. 3.6 Compressive specimen with fixture

High purity machined graphite tensile and compressive specimens of 20 mm gage diameter have been tested as per ASTM C-749 and ASTM C-695 for assessing the bimodular behavior. The tensile test specimen with fixture train is shown in Fig. 3.5 while for compressive cylindrical specimen is presented in Fig. 3.6.

The gauge length of tensile specimen is 80 mm and for compression specimen is 40 mm (ASTM C695-15 2015; ASTM C749 −15 2015). Proper care and specimen protection has been invoked during the testing for determining appropriate cross head speed so that the specimen should not break at the fixture clamp during tensile loading. Twenty specimens from each category are tested at room temperature using INSTRON UTM and the results are recorded for assessing the bimodular behaviour. Utmost care has been taken for preparing the specimens as per ASTM standard with reference to surface finish and planeness of the specimens within the tolerance values. A crosshead speed of 0.2 mm/min has been maintained throughout the testing.

The stress-strain plot is drawn using the DIC procedures. The correct value of Young's Modulus of elasticity is calculated by the linear fit of data points obtained in Digital image co-relation. The slope of the linear fit gives the modulus value. The details can be found elsewhere in ASTM E 111. The stress-strain plot for the tension specimen is represented in the Fig. 3.7.

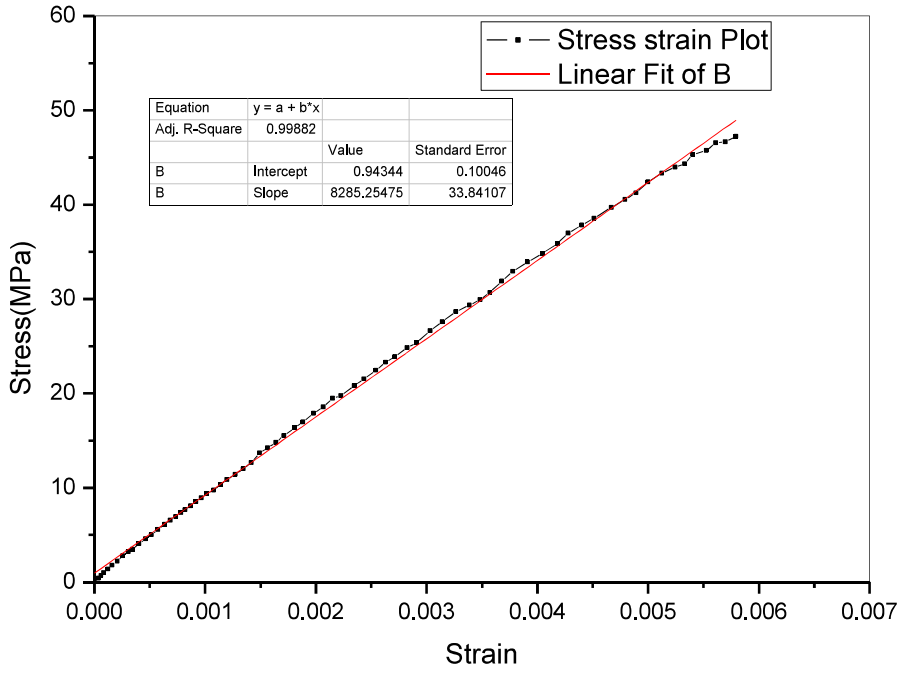

Fig. 3.7 Stress-strain plot for large tensile test (specimen no. 01) from digital image co-relation

The experimental results for the breaking stress, strain at break, extension at break and breaking load for large tensile specimen (diameter 20 mm, Gauge length 80 mm) tested according to ASTM: C-749 and tabulated in the Table 3.1. Similarly for the compressive stress-strain plot is represented in the Fig. 3.8, by using the DIC procedures. And the experimental test results for the breaking stress, strain at break, extension at break and breaking load for compressive

specimens (diameter 20 mm, Gauge length 40 mm) tested according to ASTM: C-695 and tabulated in the Table 3.2.

Table 3.1: Breaking stress, strain at break, extension at break and breaking load for large tensile specimen (diameter 20 mm, Gauge length 80 mm) tested according to ASTM: C-749.

	Extension at break with fixture	Extension at break	Breaking load	Strain at break	Breaking stress
	(mm)	(mm)	(N)	(mm/mm)	(Mpa)
Sample1	4.012	0.46	14839.6	0.0058	47.261
Sample2	3.832	0.44	14992.2	0.0056	47.746
Sample3	3.832	0.44	14520.6	0.0055	46.244
Sample4	3.745	0.43	14520.6	0.0054	46.244
Sample5	3.929	0.45	15310.6	0.0057	48.760
Sample6	3.319	0.38	12900.3	0.0048	41.084
Sample7	3.832	0.44	14190.2	0.0055	45.192
Sample8	3.842	0.44	14500.5	0.0056	46.180
Sample9	3.949	0.45	14966.1	0.0057	47.663
Sample10	3.939	0.45	15360.5	0.0057	48.919
sample11	4.026	0.46	15519.7	0.0058	49.426
sample12	4.14	0.48	16144.9	0.0061	51.417
sample13	4.16	0.48	16131.4	0.006	51.374
sample14	3.765	0.43	14781.5	0.0054	47.075
sample15	4.325	0.5	17001.8	0.0063	54.146
sample16	4.036	0.46	15482.3	0.0058	49.307
sample17	4.17	0.48	16293.7	0.006	51.891
Sample18	3.822	0.44	15061.6	0.0055	47.967
Sample19	3.812	0.44	15051.2	0.0056	47.934
Sample20	4.026	0.46	15377.2	0.0058	48.972

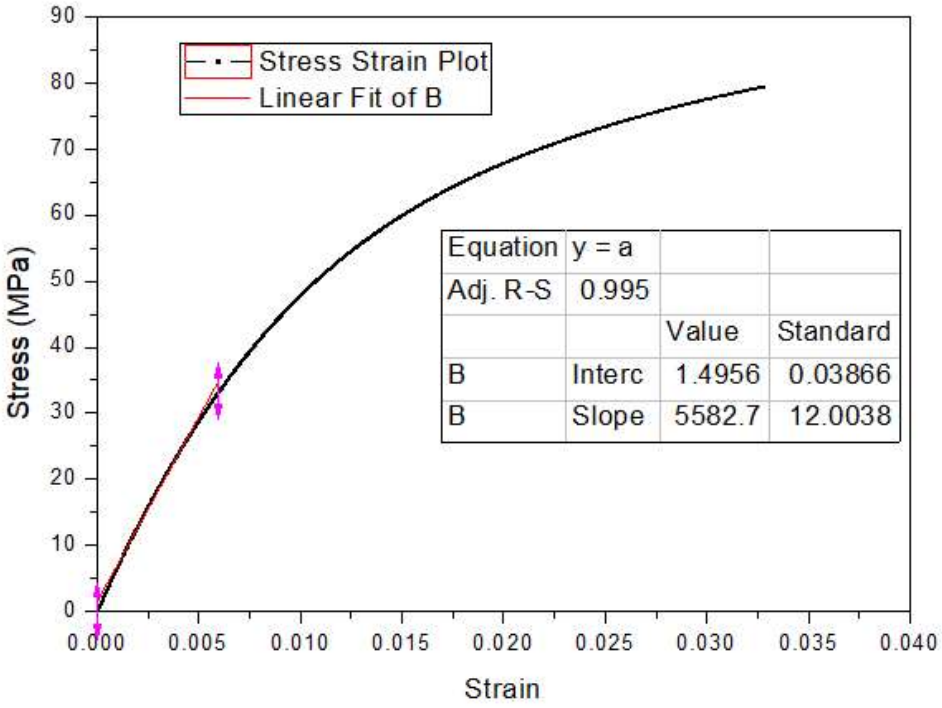

Fig. 3.8: Stress-strain plot for large compressive test (specimen no. 01) from digital image co-relation

The stress strain plot is drawn by the data points found from the digital image co-relation. For the estimation of Modulus of elasticity, the initial chord modulus has been taken from the strain range (0 to 0.006 mm/mm) by using ASTM E111. The reason behind that is maximum fracture strain has been observed is .006 mm/mm. The fracture in the flexural condition most of the ceramics materials has been initiated in tensile region, because the compressive strength is much higher than the tensile strength. The bimodular ratio has been provided by ratio of the average of Modulus of elasticity in tension and compression.

Table 3.2: Breaking stress, strain at break, extension at break and breaking load for compressive specimen (diameter 20 mm, length 40 mm) tested according to ASTM: C-695.

	Extension at break with fixture	Extension at break	Breaking load	Strain at break	Breaking stress
	(mm)	(mm)	(N)	(mm/mm)	(Mpa)
Sample1	1.592	1.296	24981.84	0.0324	79.56
Sample2	1.605	1.304	25298.98	0.0326	80.57
Sample3	1.589	1.292	25167.11	0.0323	80.15
Sample4	1.611	1.308	25019.52	0.0327	79.68
Sample5	1.654	1.348	26014.91	0.0337	82.85
Sample6	1.547	1.261	24306.74	0.0315	77.41
Sample7	1.631	1.332	25710.32	0.0333	81.88
Sample8	1.589	1.288	24670.98	0.0322	78.57
Sample9	1.578	1.284	24765.18	0.0321	78.87
Sample10	1.591	1.301	24771.46	0.0325	78.89
sample11	1.651	1.348	25562.74	0.0337	81.41
sample12	1.597	1.296	25041.52	0.0324	79.75
sample13	1.732	1.416	26881.54	0.0354	85.61
sample14	1.585	1.292	24903.34	0.0323	79.31
sample15	1.726	1.404	26253.54	0.0351	83.61
sample16	1.633	1.332	25697.76	0.0333	81.84
sample17	1.588	1.292	24966.14	0.0323	79.51
Sample18	1.613	1.316	25405.74	0.0329	80.91
Sample19	1.632	1.328	25459.12	0.0332	81.08
Sample20	1.635	1.332	25440.28	0.0333	81.02

3.7.1. Bimodularity Index from Tension Compression Data Set

The tensile Young's Modulus of elasticity E_T = 8.502 GPa and the compressive Young's Modulus of elasticity E_C = 5.618 GPa are evaluated according to ASTM E111 standard(ASTM E111-04 2010). "Modulus of elasticity values for tension and compression are the corresponding average value estimated from the test results for all twenty specimens tested in tension and compression and the same

has been tabulated in Table 3.3." The graphite is found to be bimodular and its bimodular index is determined as 1.51.

Table 3.3: Tension and compression test results for Young's Modulus of elasticity (ASTM E111).

Tensile Specimen	E_T (GPa)	Compressive Specimen	E_C (GPa)
Sample1	8.285	Sample1	5.582
Sample2	8.623	Sample2	5.653
Sample3	8.452	Sample3	5.624
Sample4	8.499	Sample4	5.591
Sample5	8.523	Sample5	5.673
Sample6	8.534	Sample6	5.431
Sample7	8.105	Sample7	5.745
Sample8	8.384	Sample8	5.513
Sample9	8.455	Sample9	5.534
Sample10	8.683	Sample10	5.535
Sample11	8.577	Sample11	5.712
Sample12	8.469	Sample12	5.596
Sample13	8.578	Sample13	5.656
Sample14	8.607	Sample14	5.565
Sample15	8.484	Sample15	5.656
Sample16	8.453	Sample16	5.672
Sample17	8.589	Sample17	5.578
Sample18	8.747	Sample18	5.677
Sample19	8.598	Sample19	5.689
Sample20	8.399	Sample20	5.685
Average Value of E_T	8.5022	Average Value of E_C	5.61835

3.8 Probabilistic Fracture Mechanics

The strength of nuclear graphite components is controlled by microstructure features, in addition to the sample size and geometry. For an example, a significant difference between bend and tensile strength in nuclear graphite is being observed, with the measured surface strain to failure is being higher in bending. Along with this, the relatively low notch sensitivity of nuclear graphites

was due to an effect of the stress gradient on the maximum stress developed. The effective volume under high stress might be very small relative to the microstructure scale in the presence of steep stress gradients. This implies a reduced probability of a large flaw being in this volume. Furthermore, in conditions where the maximum stress is sufficient to initiate fracture, the average strain energy within the small volume could be insufficient for fracture to propagate. Stable crack growth could therefore occur. Consequently, the Weibull modulus should not be expected to be independent of sample geometry, and may depend on the distribution of inherent flaws and their relation to the stressed volume in which they lie.

Now, it is well recognized that the great majority of mechanical failures result from a combination of fracture, fatigue, corrosion and material degradation processes. In order to maintain an acceptable level of structural integrity in large modern structures and components that are being subjected to more and more demanding service conditions, design and system engineers have shown an increasing concern over both these detrimental processes and in ways of describing and counteracting them. But, complexity and size become major obstacles when one has to perform real life tests to assess design parameters. The tests are either too costly or simply not feasible which forces the engineer to rely on data obtained from relatively simple laboratory testing of components, specimens or systems. Secondly, it is further recognized that data obtained from these tests exhibit a relatively large amount of scatter that must be associated with the material microstructure itself, i.e., with random distributions of lattice defects, impurity atoms, slip systems, crystal sizes, grain boundary parameters, and macro defects such as porosity, cracks and casting defects. All attest to the random

nature of material damage processes and suggests a probabilistic rather than a deterministic approach to the problems associated with the implementation of modern materials such as low impurity nuclear graphites in high temperature nuclear reactors. Brittle materials exhibit a scatter in their fracture strength. Literature says that such a scatter is caused by the distribution of microscopic flaws intrinsic in the material. However, many other properties, such as corrosion resistance, low thermal conductivity, etc., of this class of materials have made them very attractive for use as a structural material. One of their chief attractions is high-temperature strength and thus their structural applications have focused on heat engines, turbine blades, and reactor cores. Their brittle characteristics (linear or non-linear stress-strain behavior to fracture) and their near-zero ductility, combined with the large scatter in fracture strength, have led to a probabilistic approach for a design philosophy to be established in high risk structures.